Self-Assembly of Axially Functionalized Subphthalocyanines in Thin Films

Yi Ren,[a,b] Anna M. Hiszpanski,[a,b] Yueh-Lin Loo[a,b]

[a] Department of Chemical and Biological Engineering, Princeton University, Princeton, NJ 08544, USA;

[b] Princeton Center for Complex Materials, Princeton University, Princeton, NJ 08544, US.

EXPERIMENTS

General. All manipulations were carried out under a dry nitrogen atmosphere employing standard Schlenk techniques. Commercially available chemicals were purchased from Sigma-Aldrich and Alfa Aesar, and were, unless otherwise noted, used as-received. NMR solvents were purchased from Cambridge Isotope Laboratories. ^{1}H-NMR and ^{13}C{1H}-NMR, were recorded on Bruker Avance (III) 500 MHz spectrometers. Chemical shifts were referenced to external TMS (^{13}C, ^{1}H). High-resolution mass spectra of **SubPc-Me** and **F-SubPc-Me** were obtained on an Agilent 6220 Accurate-Mass Time-of-Flight LC/MS. We were not able to obtain high-resolution mass spectra on the other compounds as they degraded under the conditions at which they were ionized. The crystal structures of **SubPc-Me** (CCDC 1043261) and **F-SubPc-Me (**CCDC 1043260) were obtained by Dr. Sean Parkin of the X-ray Crystallography Facility at the University of Kentucky. The other compounds did not produce single crystals under the numerous growth conditions we tried. We sent our final products to Galbraith Laboratories, Inc., for elemental analyses. UV-vis experiments were carried out on a UV-vis-NIR Cary 5000 spectrophotometer. The fluorescence measurements were performed using a Hitachi F-7000 fluorescence spectrophotometer. Theoretical calculations were carried out using the GAUSSIAN 03 suite of programs.[S1] Electron mobilities were extracted from space charge limited current (SCLC) measurements[S2] on electron-only devices with aluminum electrodes. The average electron mobilities and standard deviations were extracted from testing four devices.

2D-Grazing-Incidence X-ray Diffraction (2D-GIXD) Experiments. 2D-GIXD experiments were conducted at the G1 station of the Cornell High Energy Synchrotron Source. At the G1 station, the beam was selected to be 0.05 mm tall and 1 mm wide. The width of the samples was 0.5 to 0.7 cm. The beam energy was selected with synthetic multilayer optics (W/B4C, 23.6 Å d-spacing). Scattered intensity was collected with a two-dimensional CCD detector. All 2D-GIXD images have been background subtracted, and polarization and absorption corrections were applied, though these corrections were generally small.[S3] GIXD experiments with *in-situ* heating were performed using a custom "SabreTube" furnace (Absolute Nano, Wixom, MI),[S4] which consists of a suspended heated silicon platform. The read-out temperature of the platform was calibrated against indium, tin, and lead standards, and samples were heated at 5 °C/min to the specified temperatures. Prior to collecting the 2D-GIXD image at a specific temperature, the sample was held at that temperature for 5 min. to equilibrate.

Synthesis of **SubPc-R** and **F-SubPc-R**:

In a one-necked 250-mL Schlenk flask, silver triflate (AgOTf, 1.2 mole equiv.) was added to a solution of **SubPc-Cl** and **F-SubPc-Cl** (1.0 mole equiv.) in anhydrous THF (15 mL) at room temperature. The resulting mixture was stirred under argon for 4 hours. Then the corresponding trialkoxyphenyl methanol was added to the reaction mixture dropwise at room temperature. The reaction mixture was further heated to 40-50 ºC overnight. The crude product was purified by flash chromatography using tetrahydrofuran and hexanes as eluent (from 10:90 by volume).

SubPc-Me was obtained as a red solid. ^{1}H NMR ($CDCl_3$, 500 MHz, δ): 8.82 – 8.01 (m, 6H), 7.88 – 7.86 (m, 6H), 5.58 (s, 2H), 3.60 (s, 6H), 3.56 (s, 3H), 2.56 (s, 2H) ppm. ^{13}C NMR ($CDCl_3$, 125 MHz, δ): 152.7, 151.5, 135.1, 131.0, 129.9, 122.2, 103.0, 62.2, 60.8, 55.9 ppm. HRMS: m/z = 592.2156 ($[M+H]^+$, Calcd. 592.4111). Elemental analysis calcd (%) for $C_{34}H_{25}BN_6O_4$: C 68.93, H 4.25, N 14.19; found: C 68.46, H 4.25, N 14.19.

SubPc-C6 was obtained as a red solid. ^{1}H NMR ($CDCl_3$, 500 MHz, δ): 8.81 – 8.79 (m, 6H), 7.87 – 7.85 (m, 6H), 5.52 (s, 2H), 3.65 – 3.61 (m, 6H), 2.51 (s, 2H), 1.61 – 1.55 (m, 8H), 1.39 – 1.22 (m, 16H), 0.90 – 0.83 (m, 9H) ppm. ^{13}C NMR ($CDCl_3$, 125 MHz, δ): 152.6, 151.5, 136.7, 134.4, 131.1, 129.9, 122.2, 104.4, 73.3, 68.8, 62.3, 31.7, 30.3, 29.4, 25.9, 22.8, 14.2 ppm. Elemental analysis calcd (%) for $C_{49}H_{55}BN_6O_4$: C 73.31, H 6.91, N 10.47; found: C 72.90, H 7.00, N 10.21.

SubPc-C12 was obtained as a red solid. ^{1}H NMR ($CDCl_3$, 500 MHz, δ): 8.81 – 8.79 (m, 6H), 7.87 – 7.85 (m, 6H), 5.52 (s, 2H), 3.65 – 3.62 (m, 6H), 2.51 (s, 2H), 1.66 – 1.54 (m, 6H), 1.36 – 1.33 (m, 6H), 1.24 (sbr, 48H), 0.87 – 0.83 (m, 9H) ppm. ^{13}C NMR ($CDCl_3$, 125 MHz, δ): 152.6, 151.5, 136.7, 134.4, 131.1, 129.8, 122.2, 104.4, 73.4, 68.8, 62.3, 32.1, 30.3, 29.9, 29.8(4), 29.7(7), 29.6, 29.5, 29.4(9), 26.3, 22.8, 14.3 ppm. Elemental analysis calcd (%) for $C_{67}H_{91}BN_6O_4$: C 76.26, H 8.69, N 7.96; found: C 76.06, H 8.92, N 7.70.

SubPc-C16 was obtained as a red solid. ^{1}H NMR ($CDCl_3$, 500 MHz, δ): 8.81 – 8.79 (m, 6H), 7.87 – 7.85 (m, 6H), 5.52 (s, 2H), 3.65 – 3.60 (m, 6H), 2.51 (s, 2H), 1.66-1.55 (m, 10H), 1.37 – 1.33 (m, 6H), 1.23 (sbr, 68H), 0.86 – 0.83 (m, 9H) ppm. ^{13}C NMR ($CDCl_3$, 125 MHz, δ): 152.7, 151.6, 136.8, 134.5, 131.2, 129.9, 122.3, 104.6, 73.5, 68.9, 62.4, 32.2, 30.5, 30.0, 29.9(9), 29.9(7), 29.9(5), 29.9(3), 29.8, 29.7, 29.6(3), 29.6(1), 26.4,

22.9, 14.4 ppm. Elemental analysis calcd (%) for $C_{79}H_{115}BN_6O_4$: C 77.54, H 9.47, N 6.87; found: C 77.22, H 9.82, N 6.92.

F-SubPc-Me was obtained as a red solid. ^{1}H NMR ($CDCl_3$, 500 MHz, δ): 5.61 (s, 2H), 3.72 (s, 6H), 3.64 (s, 3H), 2.65 (s, 2H) ppm. ^{13}C NMR ($CDCl_3$, 125 MHz, δ): 152.9, 148.4, 143.8 – 143.4 (m), 141.8-141.4 (m), 136.8, 133.8, 115.1, 102.9, 62.5, 60.7, 56.0 ppm. HRMS: m/z = 808.5956 ($[M+4H]^{4+}$, Calcd. 808.2967). Elemental analysis calcd (%) for $C_{34}H_{13}BF_{12}N_6O_4$: C 50.52, H 1.62, N 10.40; found: C 50.26, H 1.78, N 10.40.

F-SubPc-C6 was obtained as a red solid. ^{1}H NMR ($CDCl_3$, 500 MHz, δ): 5.53 (s, 2H), 3.78 (t, J = 6.3 MHz, 4H), 3.68 (t, J = 6.6 MHz, 2H), 2.62 (s, 2H), 1.78 – 1.59 (m, 6H), 1.48 – 1.27 (m, 18H), 0.94 – 0.86 (m, 9H) ppm. ^{13}C NMR ($CDCl_3$, 125 MHz, δ): 152.8, 148.4, 143.9 – 143.4 (m), 141.7 – 141.3 (m), 136.9, 133.2, 115.0, 104.2, 73.4, 69.0, 62.8, 31.9, 31.7, 30.4, 29.5, 25.9, 25.8, 22.8, 14.2, 14.2 ppm. Elemental analysis calcd (%) for $C_{49}H_{43}BF_{12}N_6O_4$: C 57.77, H 4.25, N 8.25; found: C 58.08, H 4.21, N 7.84.

F-SubPc-C12 was obtained as a red solid. ^{1}H NMR ($CDCl_3$, 500 MHz, δ): 5.52 (s, 2H), 3.77 (t, J = 6.5 MHz, 4H), 3.68 (t, J = 6.5 MHz, 2H), 2.61 (s, 2H) 1.76 – 1.71 (m, 4H), 1.66 – 1.61 (m, 2H), 1.46 – 1.38 (m, 6H), 1.25 (sbr, 38H), 0.87 – 0.84 (m, 9H) ppm. ^{13}C NMR ($CDCl_3$, 125 MHz, δ): 152.8, 148.4, 143.9 (br), 143.4 (br), 137.0, 133.2, 115.0, 104.2, 73.4, 69.0, 62.8, 32.1, 30.4, 29.9, 29.9, 29.8, 29.8, 29.6, 29.5, 26.3, 62.2, 22.9, 14.3 ppm. Elemental analysis calcd (%) for $C_{67}H_{79}BF_{12}N_6O_4$: C 63.31, H 6.26, N 6.61; found: C 63.18, H 6.26, N 6.46.

F-SubPc-C16 was obtained as a red solid. ^{1}H NMR ($CDCl_3$, 500 MHz, δ): 5.52 (s, 2H), 3.79 (t, J = 6.5 MHz, 4H), 3.68 (t, J = 6.5 MHz, 2H), 2.62 (s, 2H) 1.76 – 1.70 (m, 4H), 1.66 – 1.61 (m, 2H), 1.45 – 1.41 (m, 6H), 1.23 (sbr, 787H), 0.86 – 0.83 (m, 9H) ppm. ^{13}C NMR ($CDCl_3$, 125 MHz, δ): 152.8, 148.4, 143.8 – 143.4 (m), 141.7 – 141.3 (m), 137.0, 133.2, 129.9, 115.1, 104.2, 73.4, 69.1, 62.8, 32.1, 30.4, 29.9, 29.8, 29.8, 29.5, 29.5, 26.3, 26.2, 22.8, 14.3 ppm. Elemental analysis calcd (%) for $C_{79}H_{103}BF_{12}N_6O_4$: C 65.92, H 7.21, N 5.84; found: C 65.89, H 7.35, N 5.79.

Figure S1. ^{1}H NMR spectrum of **SubPc-Me** in $CDCl_3$.

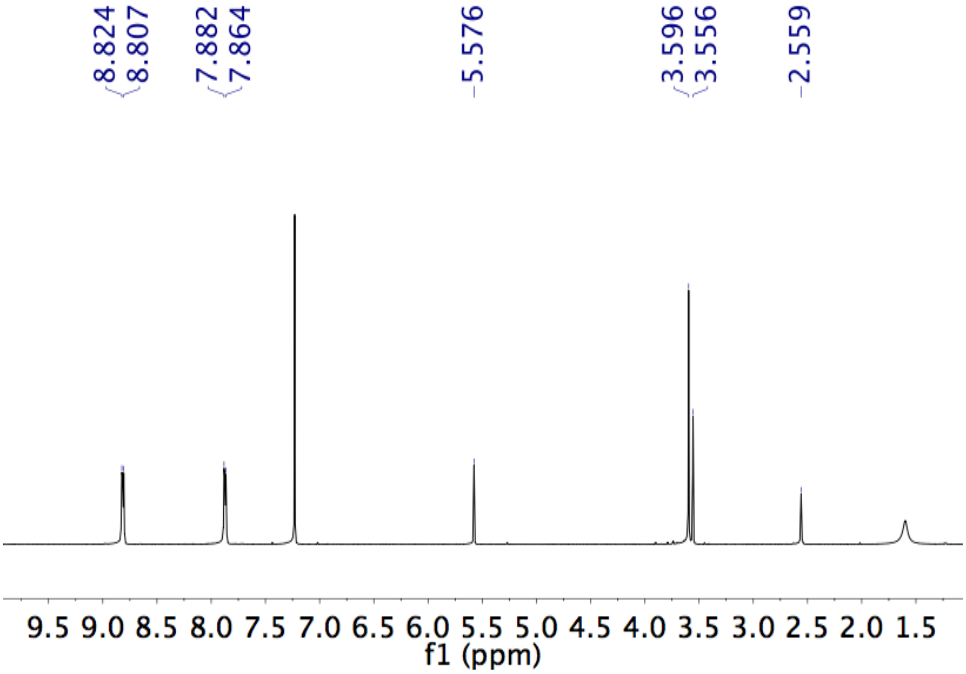

Figure S2. ^{13}C APT NMR spectrum of **SubPc-Me** in $CDCl_3$.

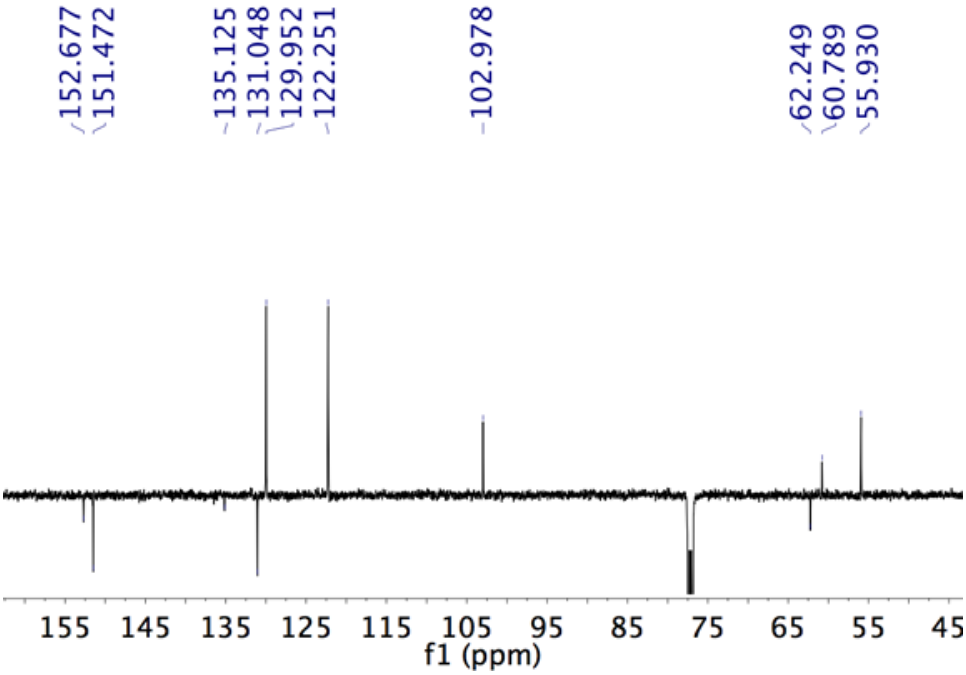

Figure S3. ^{1}H NMR spectrum of **SubPc-C6** in $CDCl_3$.

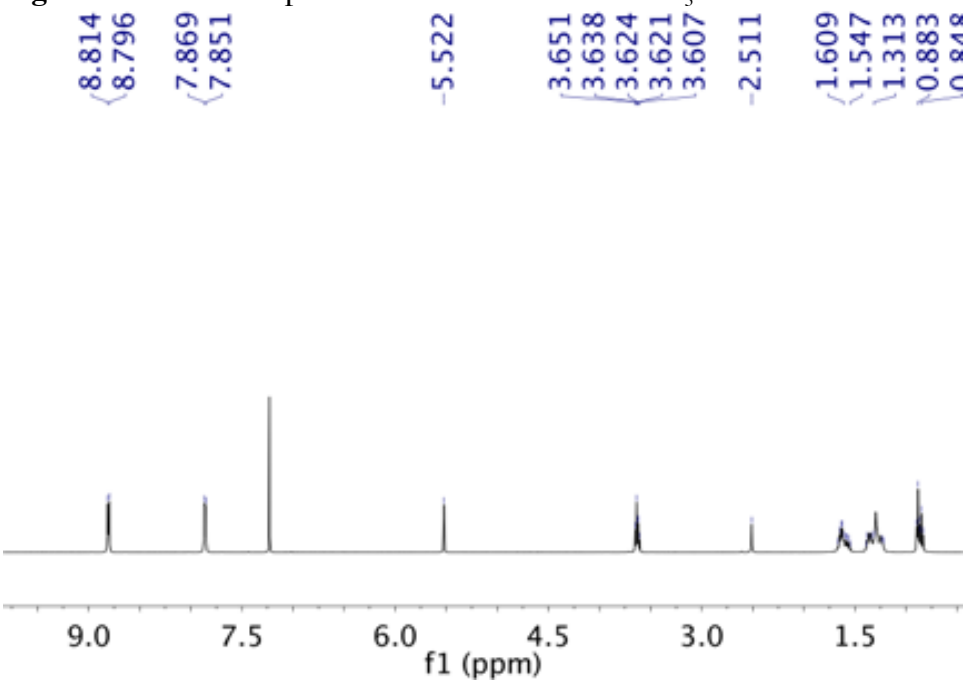

Figure S4. ^{13}C NMR APT spectrum of **SubPc-C6** in $CDCl_3$.

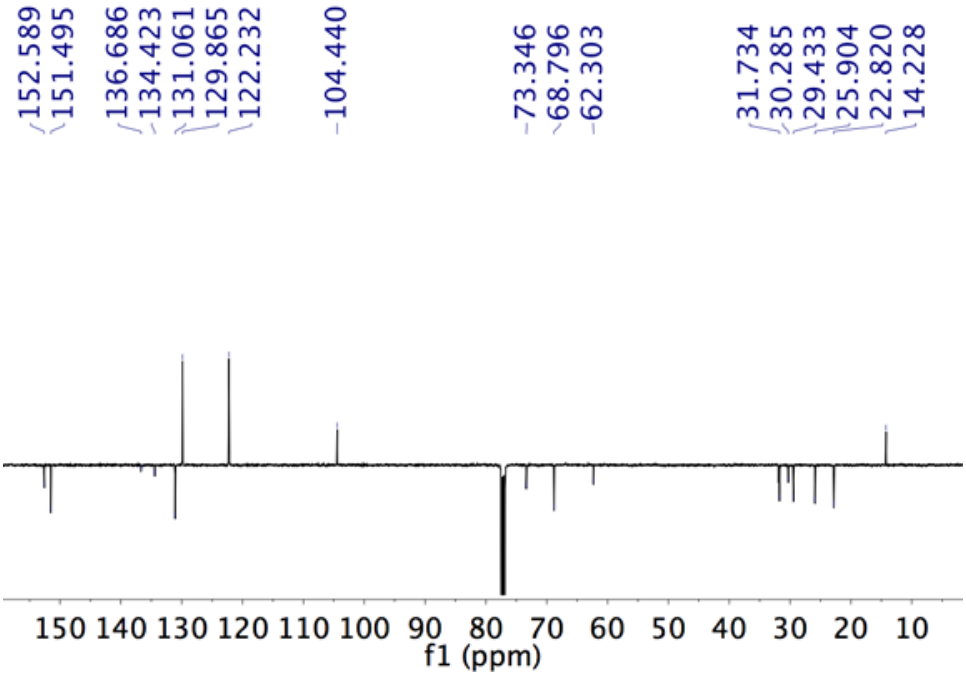

Figure S5. ^{1}H NMR spectrum of **SubPc-C12** in $CDCl_3$.

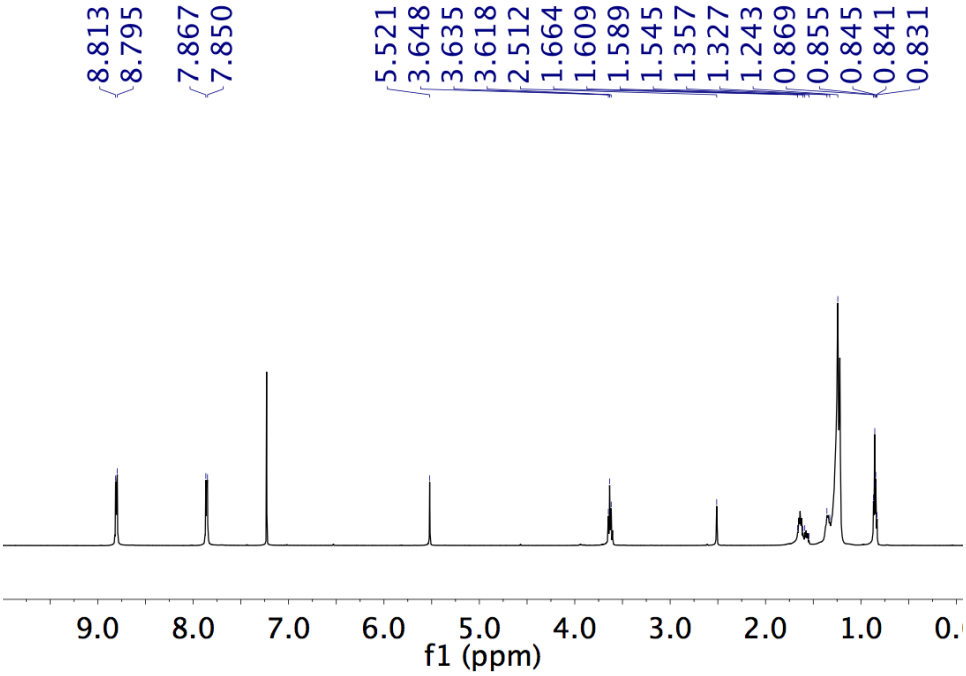

Figure S6. ^{13}C APT NMR spectrum of **SubPc-C12** in $CDCl_3$.

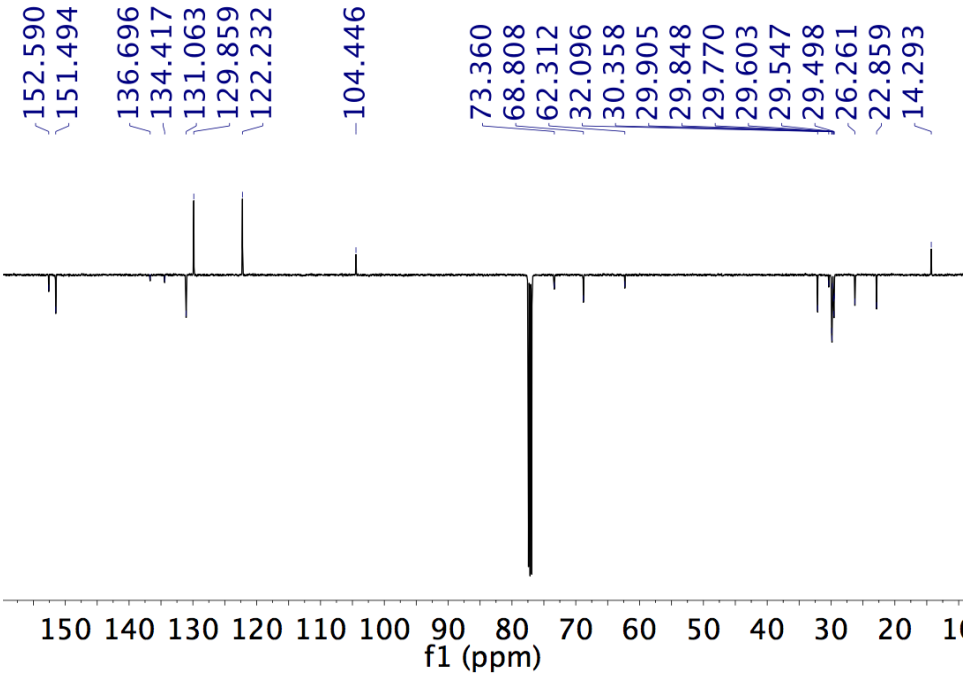

Figure S7. ^{1}H NMR spectrum of **SubPc-C16** in $CDCl_3$.

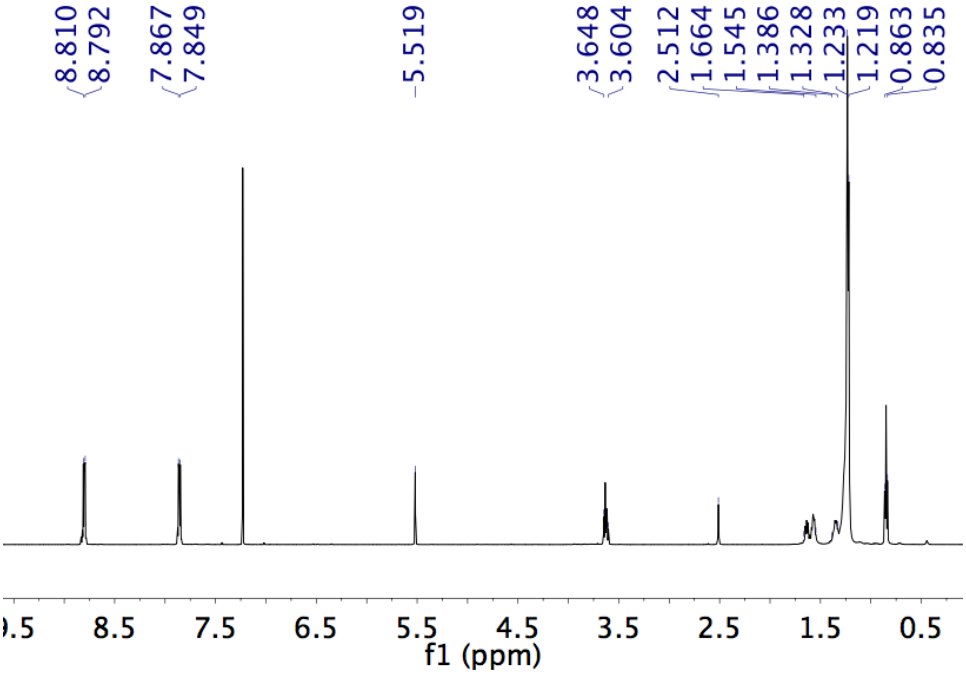

Figure S8. ^{13}C APT NMR spectrum of **SubPc-C16** in $CDCl_3$.

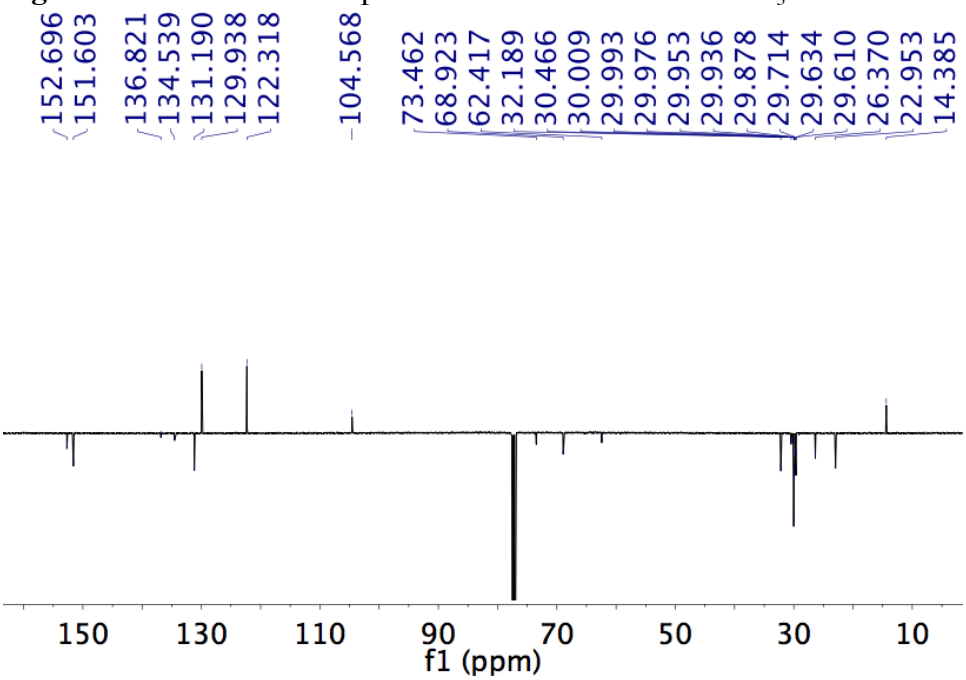

Figure S9. ^{1}H NMR spectrum of **F-SubPc-Me** in $CDCl_3$

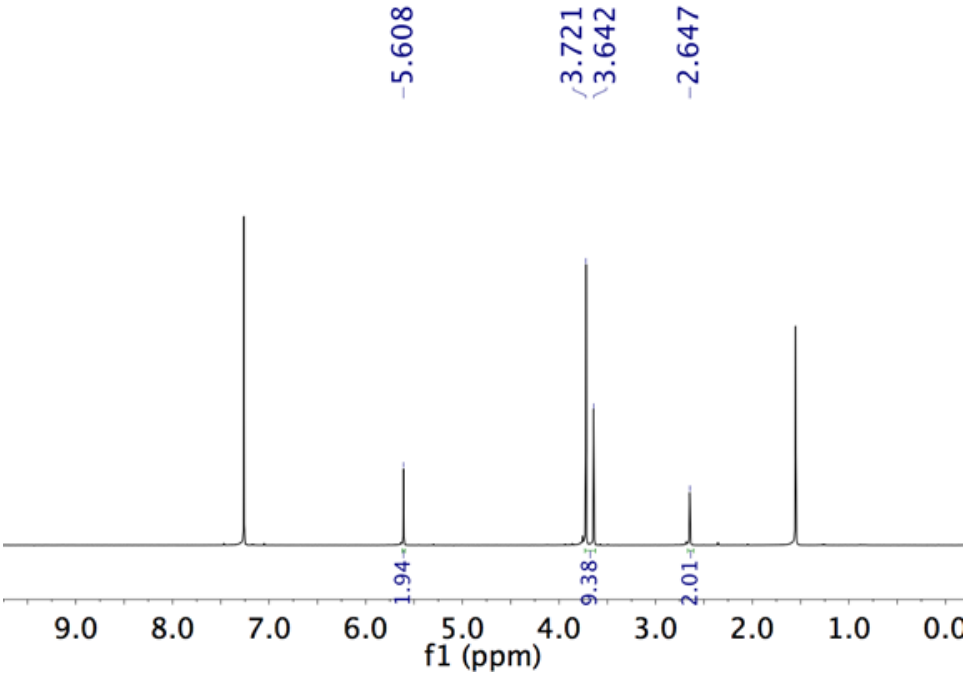

Figure S10. ^{13}C APT NMR spectrum of **F-SubPc-Me** in $CDCl_3$

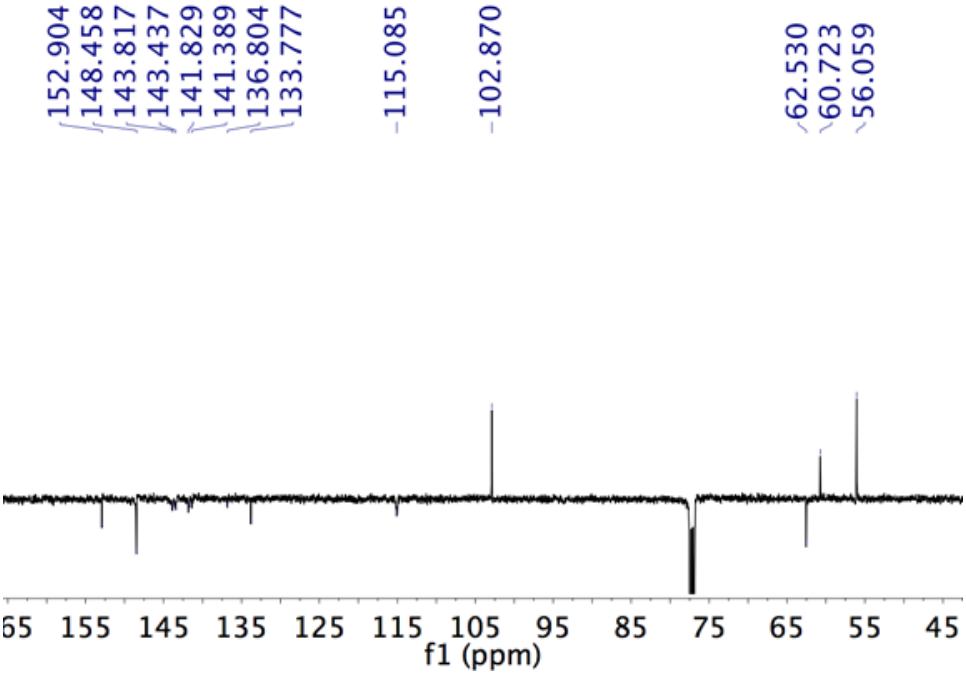

Figure S11. ^{1}H NMR spectrum of **F-SubPc-C6** in $CDCl_3$.

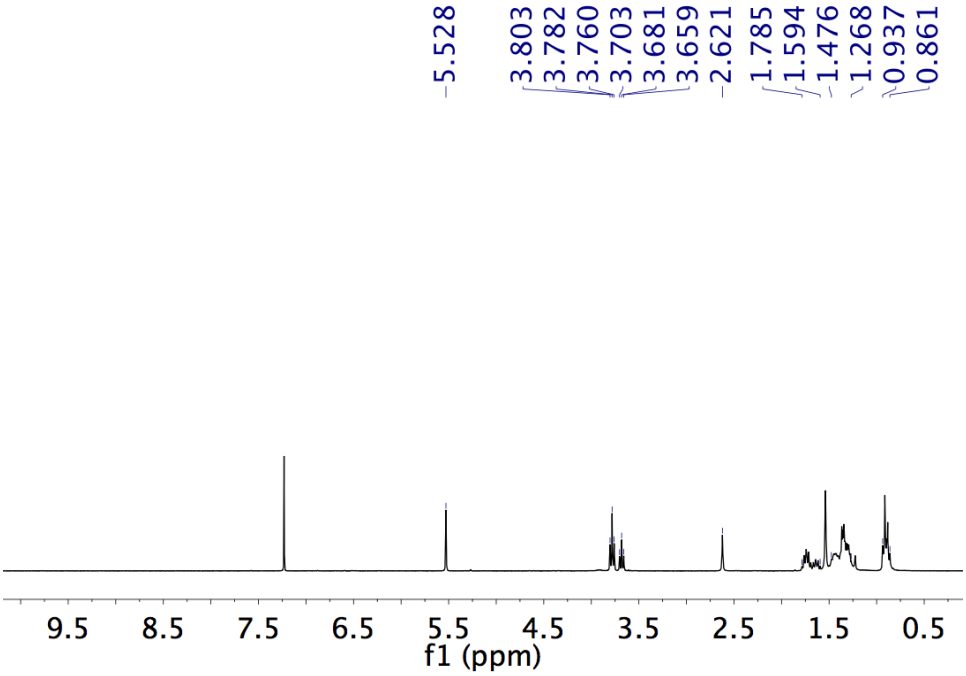

Figure S12. ^{13}C APT NMR spectrum of **F-SubPc-C6** in $CDCl_3$.

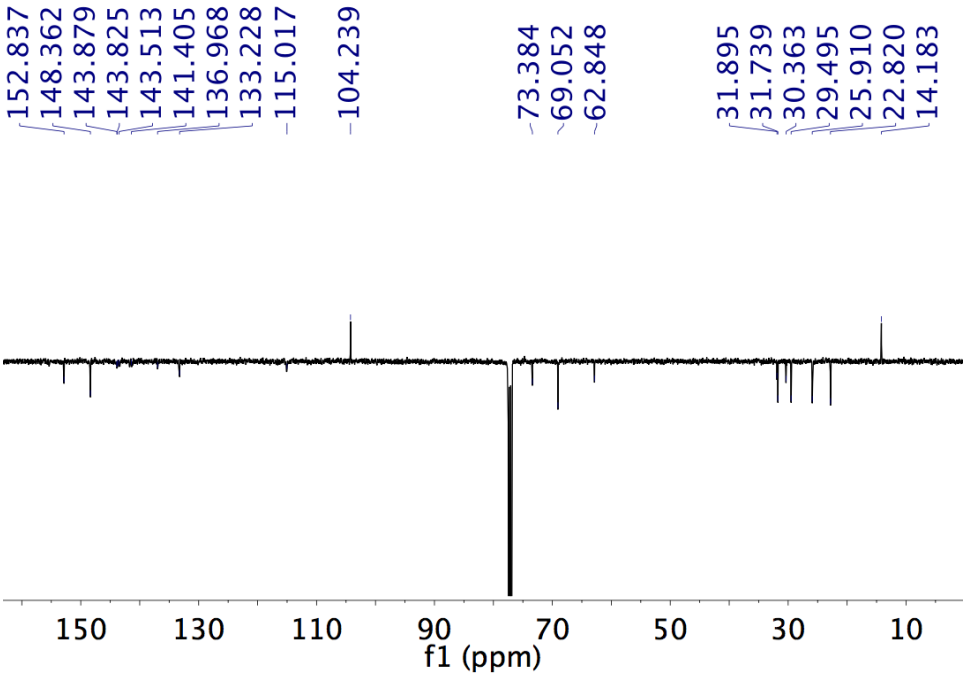

Figure S13. ^{1}H NMR spectrum of **F-SubPc-C12** in $CDCl_3$.

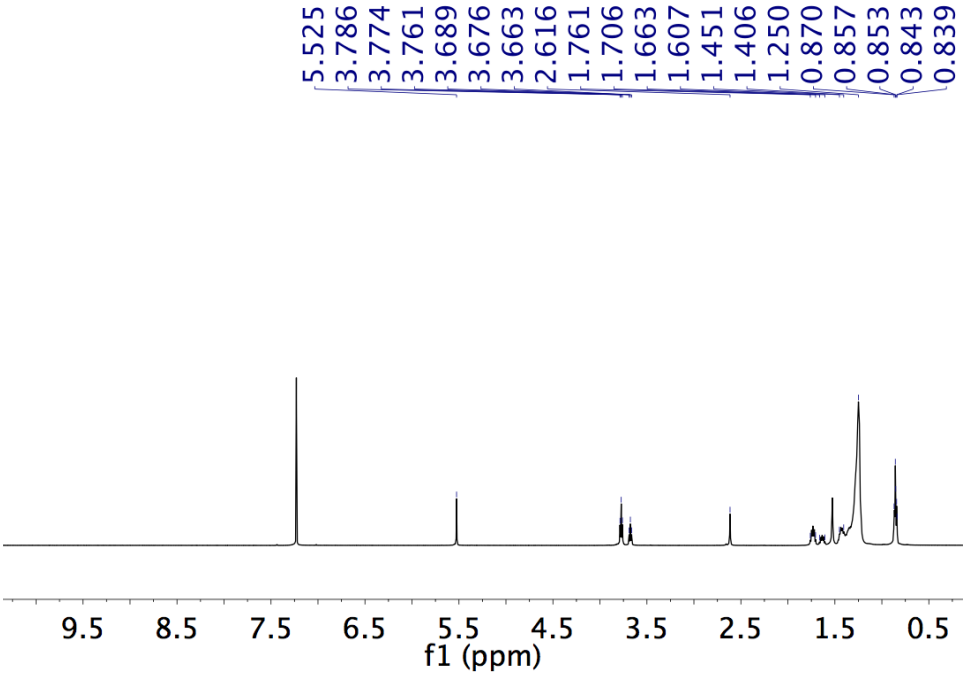

Figure S14. ^{13}C APT NMR spectrum of **F-SubPc-C12** in $CDCl_3$.

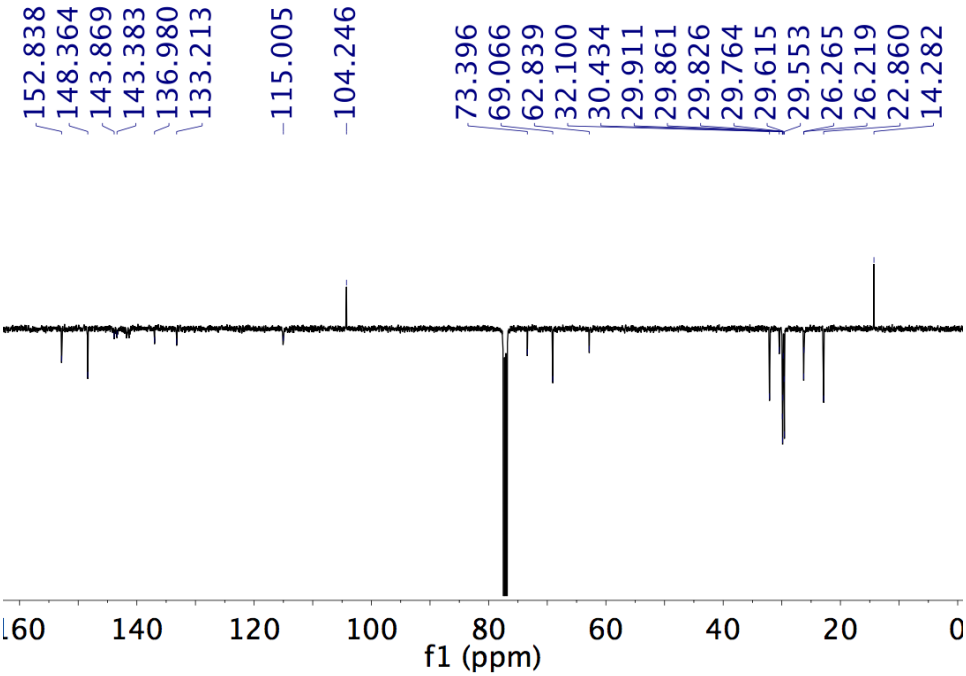

Figure S15. ^{1}H NMR spectrum of **F-SubPc-C16** in $CDCl_3$.

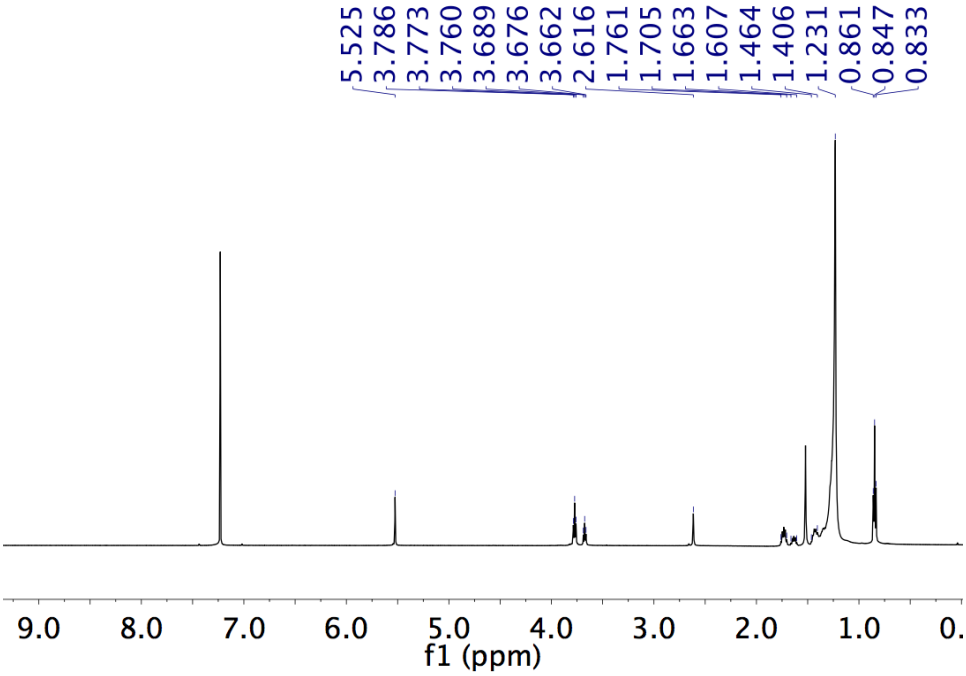

Figure S16. ^{13}C APT NMR spectrum of **F-SubPc-C16** in $CDCl_3$.

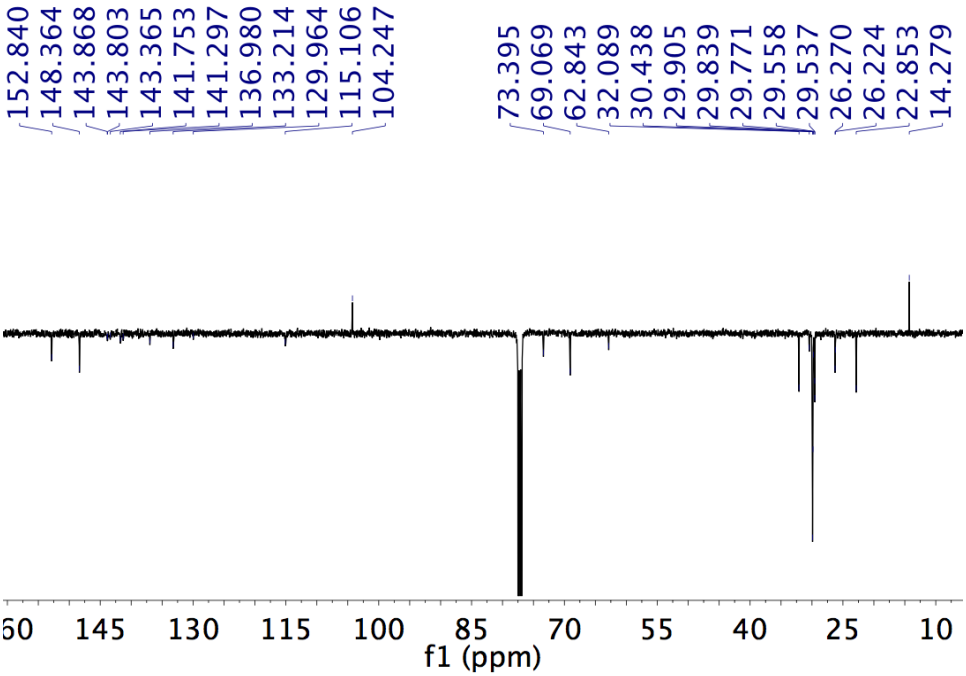

Figure S17. Crystal structures of (a, b, c) **SubPc-Me** and (d, e, f) **F-SubPc-Me**.

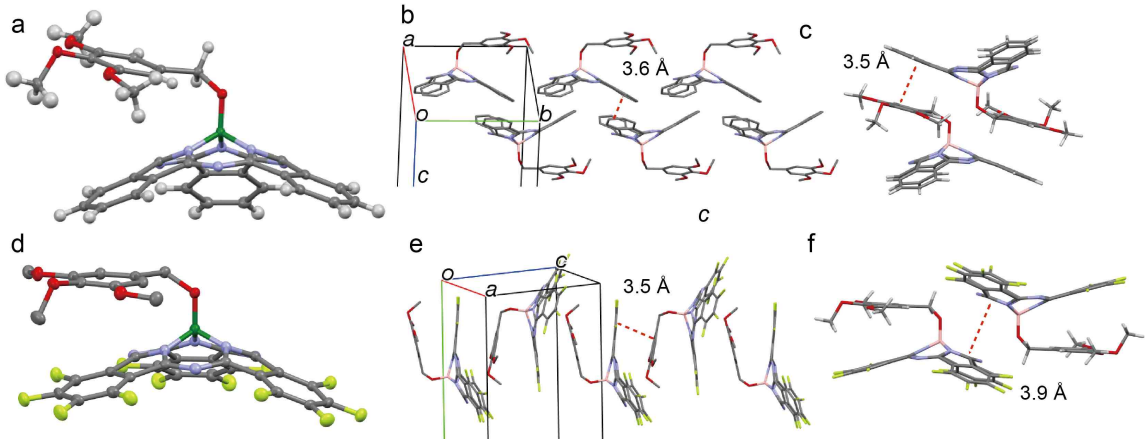

Figure S18. Frontier molecular orbitals of **SubPc-Me** (left) and **F-SubPc-Me** (right) obtained by TD-DFT calculations at the level of B3LYP/6-31G(d,p). Crystal structures of **SubPc-Me** and **F-SubPc-Me** were used to generate input files.

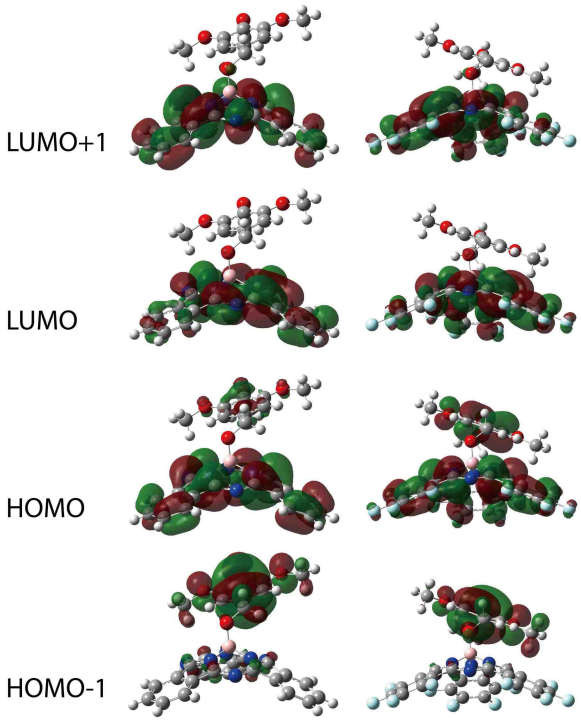

Based on the TD-DFT calculations (Table S2), the LUMO (HOMO) and LUMO-1 (HOMO+1) for both **SubPc-Me** and **F-SubPc-Me** are degenerated. That the electrons are localized on the trimethyoxylbenzyloxyl tail in the HOMO-1 of SubPc-Me and F-SubPc-Me and on the SubPc core in their LUMO and LUMO+1 are evidence for intramolecular charge transfer in these compounds.

Figure S19. (a) DSC trace of **SubPc-C6** (2nd heat and 1st cool) and (b, c, d) 2D-GIXD images of **SubPc-C6** acquired at different temperatures upon heating.

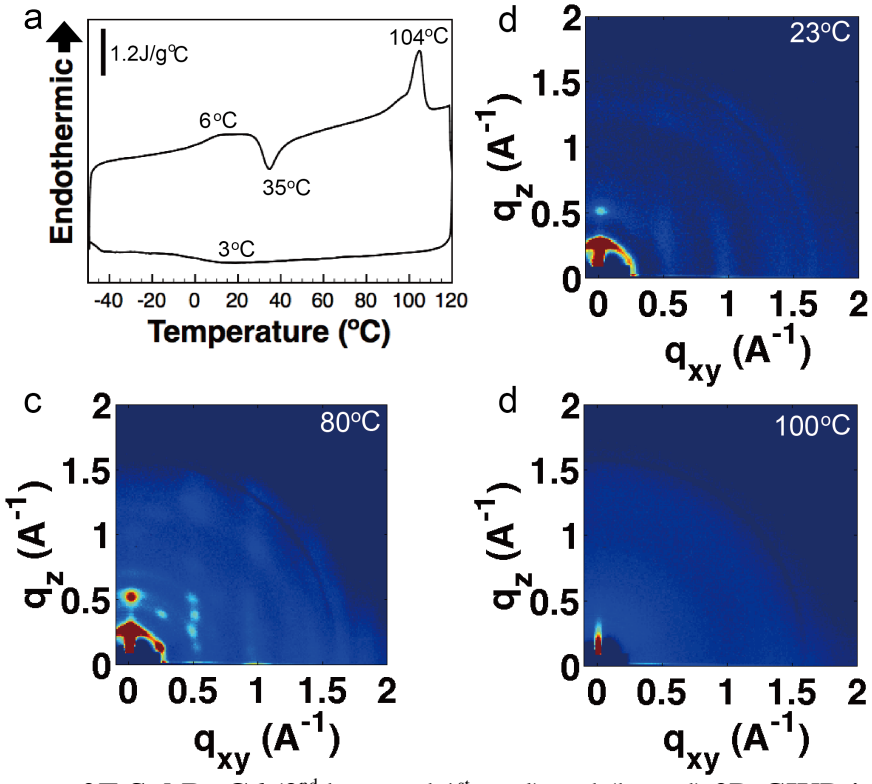

Figure S20. (a) DSC trace of **F-SubPc-C6** (2nd heat and 1st cool) and (b, c, d) 2D-GIXD images of **F-SubPc-C6** acquired at different temperatures.

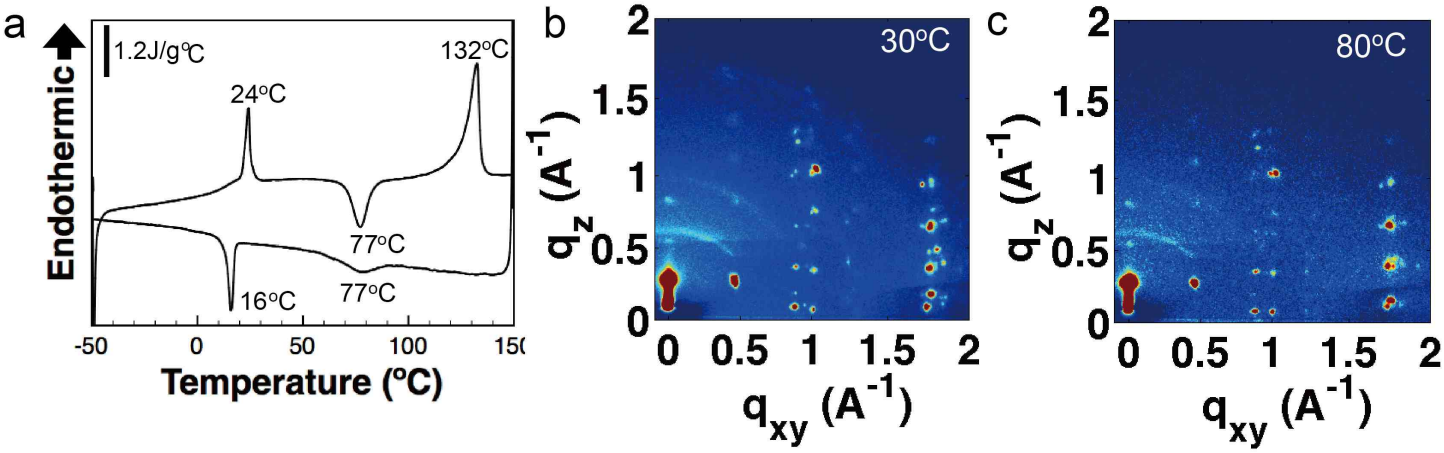

Figure S21. 2D-GIXD images of **SubPc-C12** acquired at different temperatures upon heating.

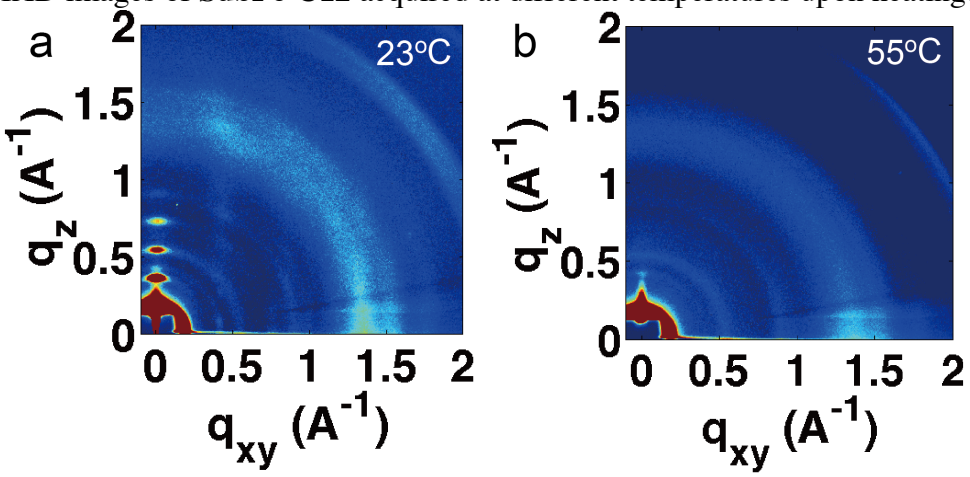

Figure S22. (a) DSC trace of **F-SubPc-C12** (2nd heat and 1st cool) and (b, c, d) 2D-GIXD images of **F-SubPc-C12** acquired at different temperatures upon heating.

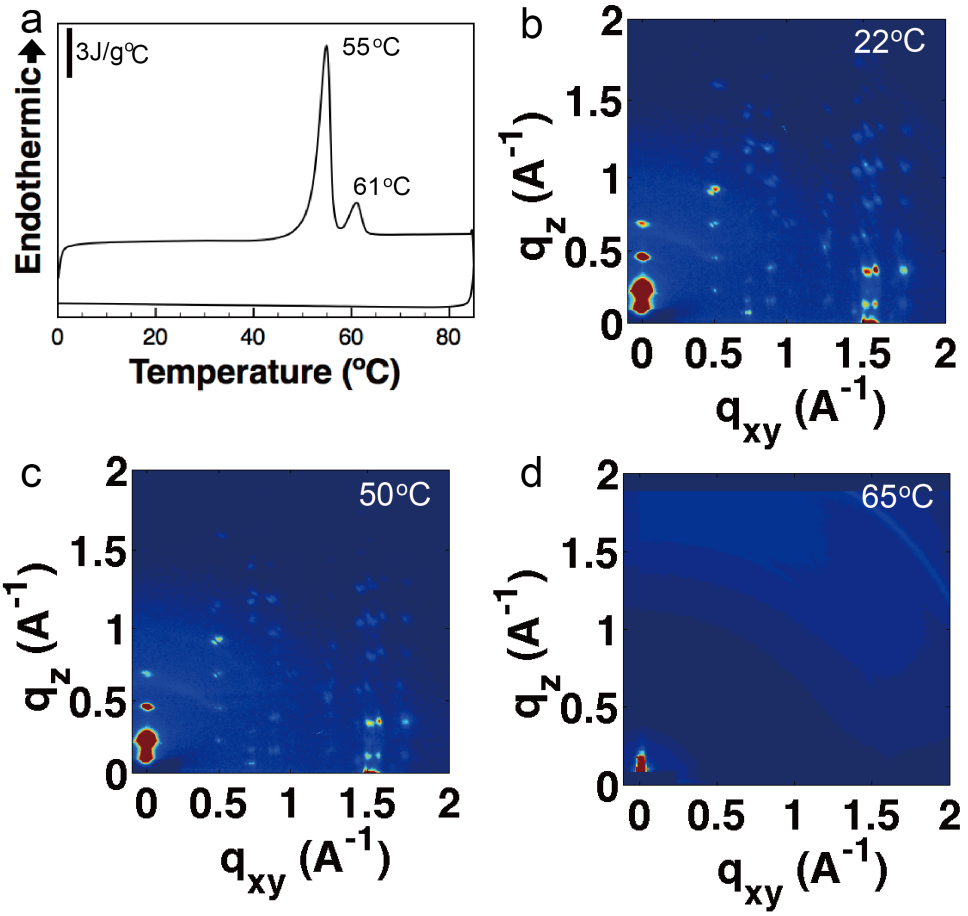

Figure S23. 2D-GIXD images of **SubPc-C16** acquired at different temperatures upon heating.

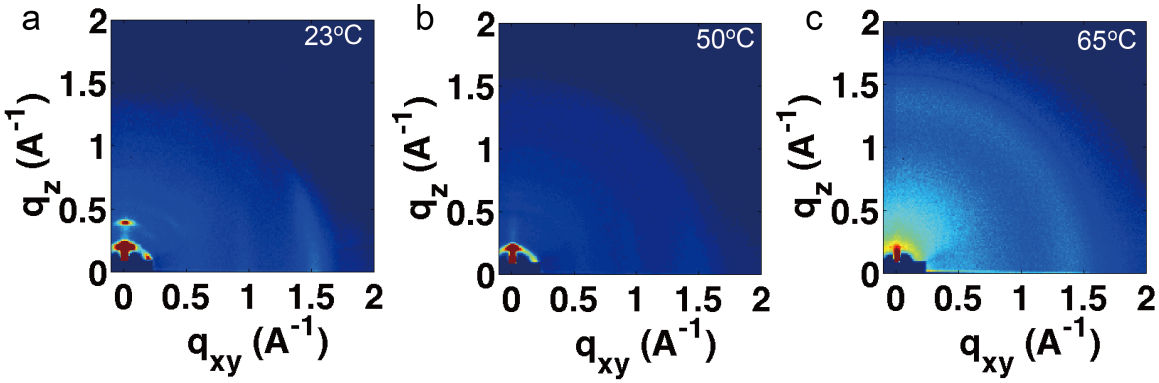

Figure S24. (a) DSC trace of **F-SubPc-C16** (2nd heat and 1st cool) and (b, c) 2D-GIXD images of **F-SubPc-C16** acquired at different temperatures upon heating.

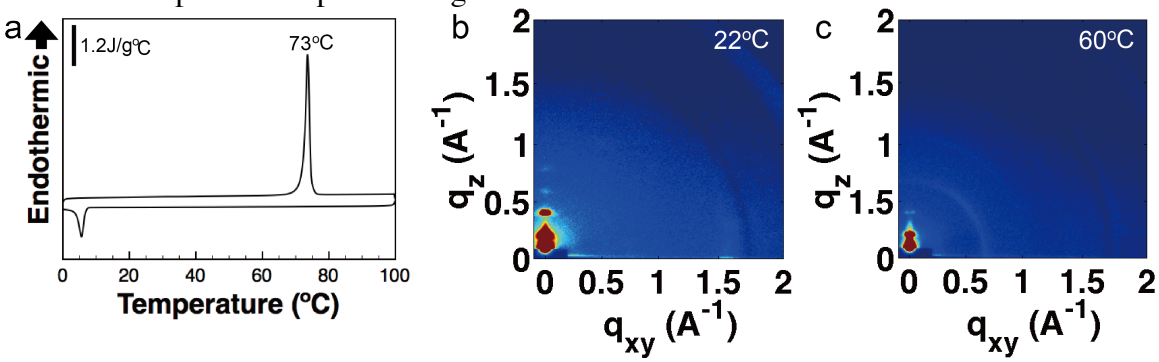

Figure S25. a) Emission spectra of (a) **SubPc-C6**; (b) **SubPc-C12**; (c) **SubPc-C16**; (d) **F-SubPc-C6**; (e) **F-SubPc-C12**; (f) **F-SubPc-C16** (black: without $PC_{71}BM$; red: with $PC_{71}BM$).

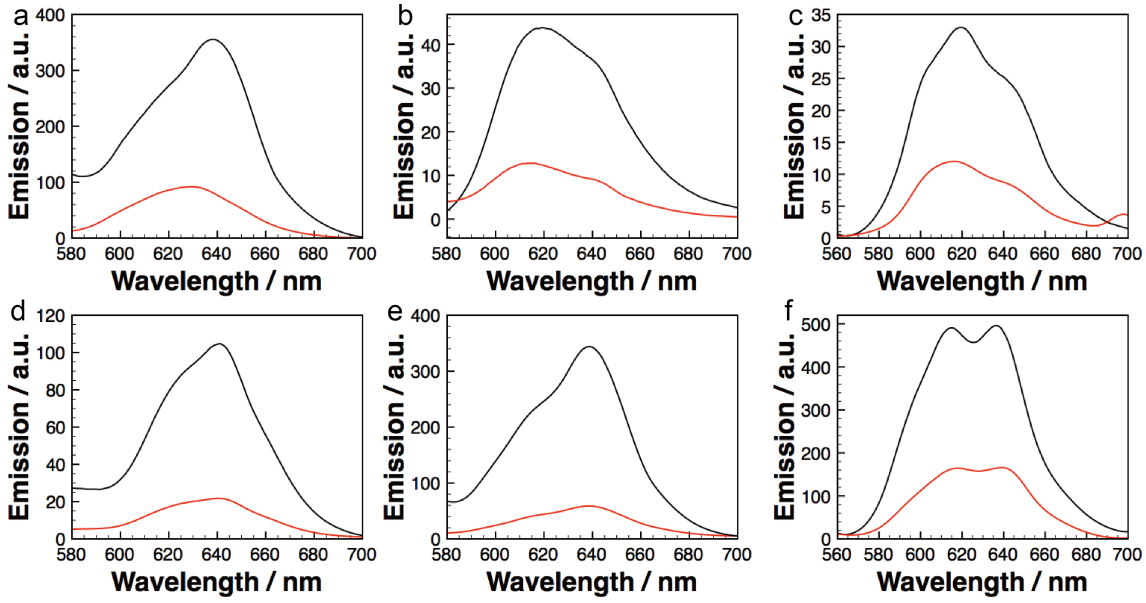

Table S1. Photophysical data of trialkoxybenzyloxyl SubPcs and F-SubPcs.

Compound	λ_{abs} [a] [nm]	λ_{em} [b] [nm]	ϕ_{FL} [d]
SubPc-Me	557	568	0.017
SubPc-C6	557	568	0.017
SubPc-C12	557	568	0.019
SubPc-C16	557	568	0.020
F-SubPc-Me	570	585	0.007
F-SubPc-C6	570	585	0.005
F-SubPc-C12	570	585	0.009
F-SubPc-C16	570	585	0.009

[a] Absorption maximum measured in heptane. [b] Emission maximum measured in heptane. [c] Fluorescence quantum yield measured in heptane relative to Rhodamine 6G.

Table S2. Theoretical data of for **SubPc-Me** and **F-SubPc-Me**.[a]

Compound	$S_0 \Rightarrow S_1$	Transition Energy of $S_0 \Rightarrow S_1$ [nm]	f [b]
SubPc-Me	HOMO-1⇒LUMO HOMO-1⇒LUMO+1 HOMO⇒LUMO	516.06 (2.40 eV)	0.0433
F-SubPc-Me	HOMO-1⇒LUMO HOMO⇒LUMO+1 HOMO⇒LUMO	588.63 (2.10 eV)	0.005

[a] TD-DFT calculated at the level of TD-B3LYP/6-31G(d,p); [b] oscillator strength.

References:

S1. Frisch, M. J.; Trucks, G. W.; Schlegel, H. B.; Scuseria, G. E.; Robb, M. A.; Cheeseman, J. R.; Montgomery, Jr., J. A.; Vreven, T.; Kudin, K. N.; Burant, J. C.; Millam, J. M.; Iyengar, S. S.; Tomasi, J.; Barone, V.; Mennucci, B.; Cossi, M.; Scalmani, G.; Rega, N.; Petersson, G. A.; Nakatsuji, H.; Hada, M.; Ehara, M.; Toyota, K.; Fukuda, R.; Hasegawa, J.; Ishida, M.; Nakajima, T.; Honda, Y.; Kitao, O.; Nakai, H.; Klene, M.; Li, X.; Knox, J. E.; Hratchian, H. P.; Cross, J. B.; Bakken, V.; Adamo, C.; Jaramillo, J.; Gomperts, R.; Stratmann, R. E.; Yazyev, O.; Austin, A. J.; Cammi, R.; Pomelli, C.; Ochterski, J. W.; Ayala, P. Y.; Morokuma, K.; Voth, G. A.; Salvador, P.; Dannenberg, J. J.; Zakrzewski, V. G.; Dapprich, S.; Daniels, A. D.; Strain, M. C.; Farkas, O.; Malick, D. K.; Rabuck, A. D.; Raghavachari, K.; Foresman, J. B.; Ortiz, J. V.; Cui, Q.; Baboul, A. G.; Clifford, S.; Cioslowski, J.; Stefanov, B. B.; Liu, G.; Liashenko, A.; Piskorz, P.; Komaromi, I.; Martin, R. L.; Fox, D. J.; Keith, T.; Al-Laham, M. A.; Peng, C. Y.; Nanayakkara, A.; Challacombe, M.; Gill, P. M. W.; Johnson, B.; Chen, W.; Wong, M. W.; Gonzalez C.; Pople, J. A. Gaussian 03, Revision E. 01, Gaussian Inc.: Wallingford, CT, 2007.

S2. (a) Mihailetchi, V. D.; van Duren, J. K. J.; Blom, P. W. M.; Hummelen, J. C.; Janssen, R. A. J.; Kroon, J. M.; Rispens, M. T.; Verhees, W. J. H.; Wienk, M. M. Electron Transport in a Methanofullerene, *Adv. Funct. Mater.* **2003**, *13*, 43-46. (b) Blom, P. W. M.; deJong, M. J. M.; vanMunster, M. G. Electric-Filed and Temperature Dependence of the Hole Mobility in Poly(p-Phenylene vinylene). *Phys. Rev. B* **1997**, *55*, 656-659.

S3. Hiszpanski, A. M.; Lee, S. S.; Wang, H.; Woll, A. R.; Nuckolls, C.; Loo, Y.-L. Post-Deposition Processing Methods to Induce Preferential Orientation in Contorted Hexabenzocoronene Thin Films, *ACS Nano*. **2013**, *7*, 294-300.

S4. van Laake, L.; Hart, A. J.; Slocum A. H. Suspended Heated Silicon Platform for Rapid Thermal Control of Surface Reactions with Application of Carbon Nanotube Synthesis. *Rev. Sci. Instrum.* **2007**, *78*, 083901.